COMMON-REFLECTION-SURFACE STACK: ACCOUNTING FOR CONFLICTING DIP SITUATIONS BY CONSIDERING ALL POSSIBLE DIPS

MEHRDAD SOLEIMANI[1], IRADJ PIRUZ[1], JÜRGEN MANN[2], PETER HUBRAL[2]

[1] *Faculty of Mining, Petroleum and Geophysics, Shahrood University of Technology, Shahrood, Iran.*
[2] *Geophysical Institute, University of Karlsruhe (TH), Hertzstr. 16, 76187 Karlsruhe, Germany.*
msoleimani@shahroodut.ac.ir

(Received January 8, 2009; revised version accepted March 24, 2009)

ABSTRACT

Soleimani, M., Piruz, I., Mann, J. and Hubral, P., 2009. Common-Reflection-Surface stack: accounting for conflicting dip situations by considering all possible dips. *Journal of Seismic Exploration*, 18: 271-288.

The common-reflection-surface stack was originally introduced as a data-driven method to simulate a zero-offset section from 2D seismic reflection prestack data. The principle of the CRS stack is to sum along a surface of contributions from an entire segment of a reflector instead of a reflection point. The aim of the CRS stack is not only to provide a well-simulated zero-offset section but also to determine certain attributes of hypothetical wavefronts at the acquisition surface. The CRS stack is independent of explicit velocity information and only requires the near-surface velocity in case a geometrical interpretation of its stacking parameters is desired. An important aspect of the method is that the estimated parameters are kinematic wavefield attributes which provide significant information on subsurface structures. The pragmatic search strategy of the original CRS stack implementation consists of three one-parameter searches. This implementation determines only one optimum stacking operator for each ZO sample to be simulated. Consequently, conflicting dip situations are not taken into account but only the most prominent event contributes to a particular stack sample. In one of the efforts to overcome this problem, the strategy has been extended in order to take into account up to five conflicting dips at each sample. Here, we propose a strategy which explicitly considers all possible angles and, thus, accounts for all the conflicting dips that may exist at each zero-offset sample to be simulated. This new strategy offers some advantages, e.g., it improves the continuity of events, reflections as well as diffractions, in conflicting dip situations. It also generally emphasizes diffraction events in the stacked section so that we can call it common-diffraction-surface stack. This method has the drawback that it does not give any section of wavefield attributes or coherence as, e.g., required for CRS-based tomography. Here, we processed the Sigsbee 2A synthetic data and also a real land data set with the new method and observe enhanced diffraction events and resolved conflicting dip situations. For the real data set, the definition of faults after poststack migration significantly improves.

KEYWORDS: common-reflection-surface stack, conflicting dips, coherence analysis, wavefield attributes, DMO operator.

0963-0651/09/$5.00

INTRODUCTION

The objective of seismic reflection imaging is to provide an image of the subsurface from multi-coverage seismic reflection data by enhancing genuine reflection signals and suppressing unwanted energy in the form of coherent and random ambient noise. The Common-Reflection-Surface (CRS) stack (see, e.g., Hubral, 1999; Mann, 2002; Jäger, 1999) is a data-driven imaging method to simulate a zero-offset (ZO) section. Introduced by Müller (1998) and Müller et al. (1998) as a ZO simulation method for 2D, it does not require an explicit knowledge of the macro-velocity model. The underlying model assumptions of the CRS stack method are more general than the model assumptions of, for example, Kirchhoff migration or normal moveout correction/dip moveout correction/stack, which are based on diffractors or ZO isochron segments in the subsurface, respectively. The CRS stack assumes the subsurface to be set up by reflector segments with arbitrary location, orientation, and curvature. Obviously, this subsurface model is more appropriate to describe reflectors in the subsurface than any other method based on a less general approach. The stacking operator is a second-order approximation of the kinematic reflection response of a curved interface in a laterally inhomogeneous medium. For the 2D case, the shape of the operator depends on three parameters and can be considered as the approximate reflection response of a circular reflector mirror segment, the so-called CRS (Jäger, 1999). Any contributions along any realization of this operator are tested by coherence analysis for each ZO sample, and the set of attributes which yields the highest coherence is accepted as the parameters of the optimum operator to perform the actual stack. Compared to conventional stacking techniques, the CRS stack has the potential to sum up more coherent energy of the reflection event which results in a high signal-to-noise ratio (S/N) in the simulated ZO section (e.g., Mann et al., 1999).

However, in each ZO section we can see that in some cases the events intersect each other at offset zero, e. g. when there are diffraction events which intersect many reflection events with their long tails, or bow-tie structures that intersect themselves. It is obvious that at samples where such events intersect, a single stacking operator associated with only one triplet of optimum attributes is not sufficient. Instead, a separate operator is required for each contributing event. In seismic data processing, this problem is called conflicting dip situation. Fig. 1 shows the shape of the CRS operator for a sample without conflicting dip situation, but it is evident that for other ZO samples like $\tilde{P}_0$, a single stacking operator is insufficient to capture all contributions. The problem for such samples requiring different operators is to decide how many and which operators should be used to perform the actual stack.

In the CRS stack procedure, the optimum wavefield attributes characterize the most coherent event. In the following sections, we are going to overcome

the problem of conflicting dips in the CRS stack by adapting the original search strategy and comparing the new strategy to the previous approaches to solve this problem. Finally, the new strategy will be evaluated with a synthetic data example and a real land data example.

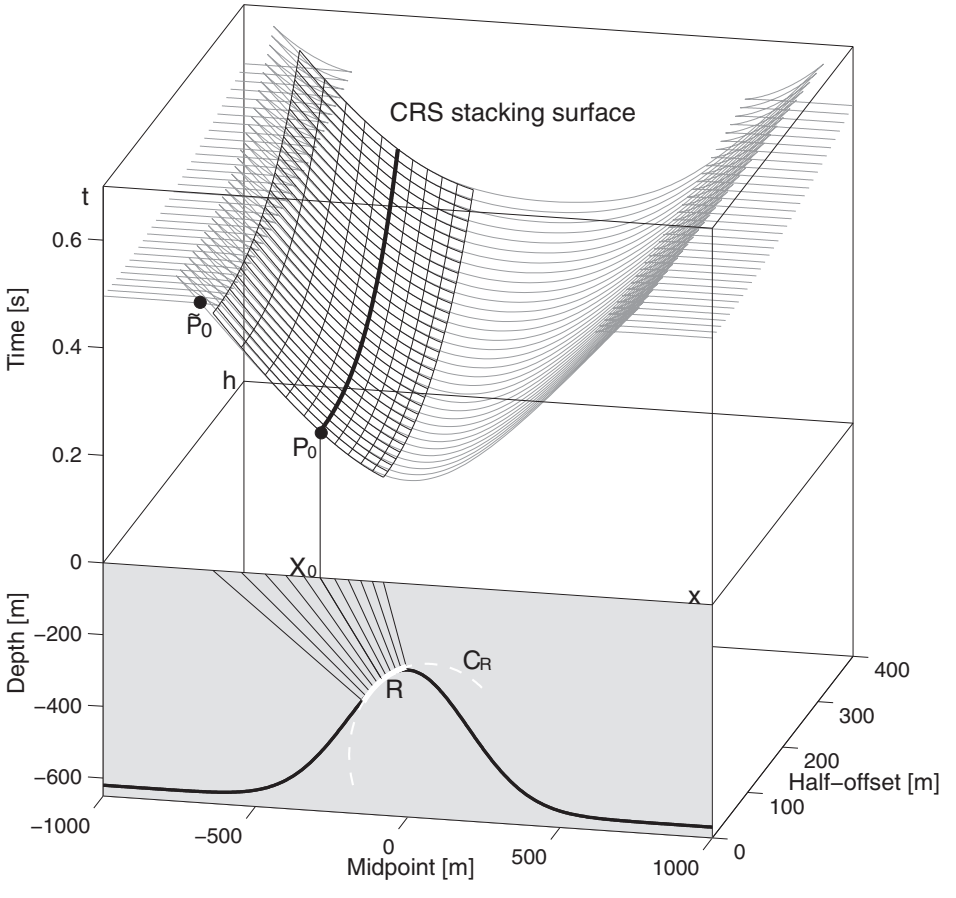

Fig. 1. The shape of the CRS operator (black surface) corresponding to a curved reflector segment (white arc) in depth. The entire reflection response is shown in gray. For point P_0, one operator is sufficient to gather the energy along the reflection event. In contrast, for point $\tilde{P}_0$, two separate operators are required, one for each branch of the reflection event (modified after Jäger, 1999).

PRAGMATIC SEARCH STRATEGY

To apply the CRS stack in an entirely data oriented way, its attributes have to be determined automatically from the prestack data (Jäger, 1999). In its original form, no initial guess is used in order to avoid any bias (although some reference functions might be quite useful in practice). The only restriction is to search for each attribute within a user-defined range and determine the best value with coherence analysis. To be on the safe side, this range should be chosen rather too large than too small (Mann, 2002). The most efficient determination of the parameters of the CRS equation

$$t_{hyp}^2(x_m,h) = [t_0 + 2\sin\alpha(x_m - x_0)/v_0]^2 + \{(2t_0\cos^2\alpha)/v_0\}[(x_m - x_0)^2/R_N + h^2/R_{NIP}] \quad , \qquad (1)$$

where R_{NIP} is the radius of the normal-incidence-point (NIP) wave, R_N is the radius of the normal wave, α is the emergence angle of the normal ray, and v_0 denotes the near-surface velocity, can be achieved if it is decomposed into three separate optimization problems with a search for one parameter in each. All attributes are defined at the emergence location $(x_0,0)$ of the normal ray.

Müller (1998) and Jäger et al. (2001) describe the complete CRS stack computation routine which involves three one-parameter searches. Optionally, a local optimization can be performed in which the initially found parameters serve as the starting point in the three-dimensional attribute domain. The optimized parameters are determined simultaneously. The optimization routine, which is very time consuming, uses the flexible polyhedron search method according to Nelder and Mead (1965). The pragmatic search strategy can be summarized as follows: automatic CMP stack, linear and hyperbolic ZO stacks, initial CRS stack, and optimization. The first step is to use eq. (1) in the CMP gathers $x_m = x_0$. In this case, the CRS operator reduces to the well-known CMP stack formula

$$t^2(h) = t_0^2 + 4h^2/v_{stack}^2 \quad \text{with} \quad v_{stack}^2 = 2R_{NIP}v_0/t_0\cos^2\alpha \quad , \qquad (2)$$

in terms of CRS attributes (e.g., Mann, 2002). For each point (x_0,t_0), we have to calculate the coherence value along hyperbolas given by eq. (2) for a whole range of stacking velocities and select the one which provides the highest coherence value. Subsequently, a stack along the CMP hyperbola parameterized by the respective stacking velocity is performed.

In the second step, we can employ the simulated ZO section of the automatic CMP stack for an attribute analysis performed with eq. (1) for $h = 0$. In this ZO section, eq. (1) only depends on α and R_N. Thus, for each point

(x_0, t_0), both optimal parameters α and R_N in the ZO section have to be found. This can be done in two one-dimensional searches by first setting $R_N = \infty$ and determining α. Having found α, R_N can be easily determined by means of a second one-dimensional search. At this point, all three parameters have been determined for each ZO sample. Thus, they can be inserted into the traveltime eq. (1) to calculate the traveltime for any combination of x_m and h. The subsequent stack along the traveltime surface is called initial CRS stack. The word "initial" is used because the CRS attributes used for this stacking serve as initial values for the optional optimization process which yields the optimized stack. It is important to note that the optimization is computationally the most expensive part. While in individual searches for the initial attributes in the CMP stack and the ZO section are performed by coherence analyses along curves, the combined search in the local optimization makes use of the entire spatial CRS stacking operator in the (x_m,h,t) prestack data domain. The final coherence section is a measure of how well the operator for a specific parameter set fits the reflection event for each considered ZO location. The higher the coherence value, the more reliable the corresponding attributes (Jäger, 1999). Note that in general the CRS operator parameterizes multiple events as well. Although the associated wavefield attributes are correct they must not be considered as attributes of primary events.

PREVIOUS IMPROVED STRATEGY

Mann (2001) introduced an extended strategy for the CRS stack to overcome the problem of conflicting dip situations. From the previous strategy, it is clear that this problem cannot be handled in the first step which is the automatic CMP stack: A stacking velocity spectrum is not very sensitive to dip and completely insensitive to its sign. Nevertheless, we can address conflicting dips in the second step, ZO search. Conflicting dips in the viewpoint of kinematic wavefield attributes simply correspond to different emergence angles $\alpha^{(i)}$. To address this problem, we have to consider more than one CRS operator, according to the number of events that contribute to a particular ZO sample. For that purpose, Mann (2002) considered additional local coherence maxima in the linear ZO stack (or slant stack). In this way, different numbers of maxima in the angle spectrum could be taken into account. In the CRS strategy, each set of attributes is analyzed separately. As a consequence, the extended strategy has to define a discrete number of contributing events at each sample. Fig. 2 shows an angle spectrum with more than one contributing event. These events are selected based on the coherence analysis performed on the CMP-stacked section. As in the previous strategy, as soon as the emergence angle is defined by the linear ZO search, in general more than one for the considered ZO location, a hyperbolic ZO search is performed to determine the curvature of the ZO events, here expressed in term of the radius of the normal wave R_N. This step will define R_N separately for all angles detected in the linear search. So, up to now,

a set of emergence angles $\alpha^{(i)}$ and their associated normal wave radii $R_N^{(i)}$, where the index i = 1,...,n numbers the i-th detected contributing event in one sample, are available.

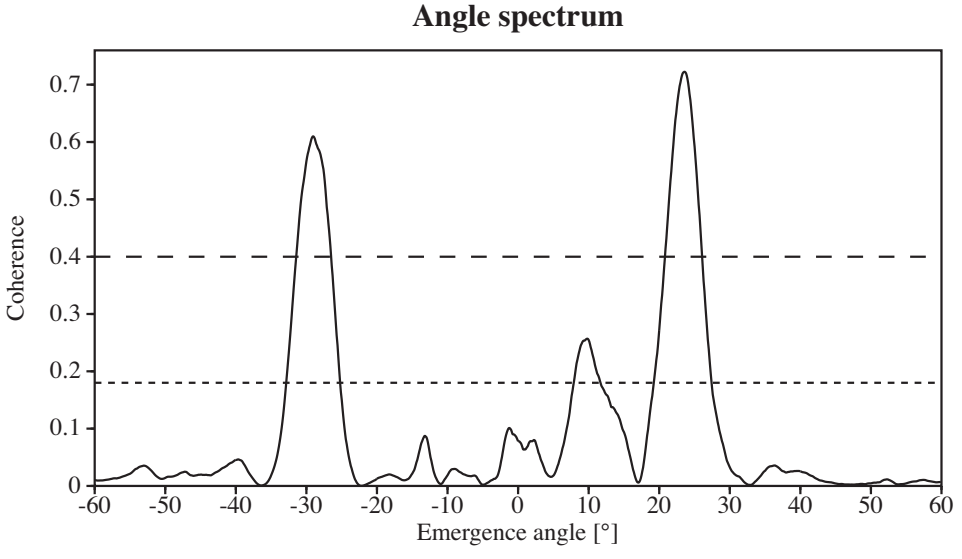

Fig. 2. Coherence as a function of emergence angle α calculated along a linear operator in the CMP stacked section for a chosen point (x_0,t_0). The three distinct maxima correspond to two diffraction events at $\approx -29°$ and $\approx 24°$ and one weak reflection event at $\approx 10°$. The long-dashed line represents the absolute threshold for the global maximum, the short-dashed line the relative threshold for global maxima chosen to identify conflicting dip situations for these particular data (from Mann, 2002).

According to eq. (2) the stacking velocity v_{stack} is related to the emergence angle α and the radius R_{NIP}. Thus, in case of only one contributing event, R_{NIP} can simply be calculated from α and v_{stack}. In conflicting dip situations this no longer holds as we are lacking the respective stacking velocities $v_{stack}^{(i)}$ for the individual events. Therefore, an additional search is required to determine the remaining attributes $R_{NIP}^{(i)}$: Mann (2002) proposed to perform this search in another sub-domain of the multi-coverage data, namely common shot (CS) and common receiver (CR) gathers. This is again a one-parameter search and provides an $R_{NIP}^{(i)}$ value for each detected event. The final step is now to perform the (optional) optimization of the attributes and to stack along the entire spatial stacking surface. This step is performed within a spatial aperture in the prestack data, the so-called CRS super gather. The flowchart of the extended strategy is depicted in Fig. 3.

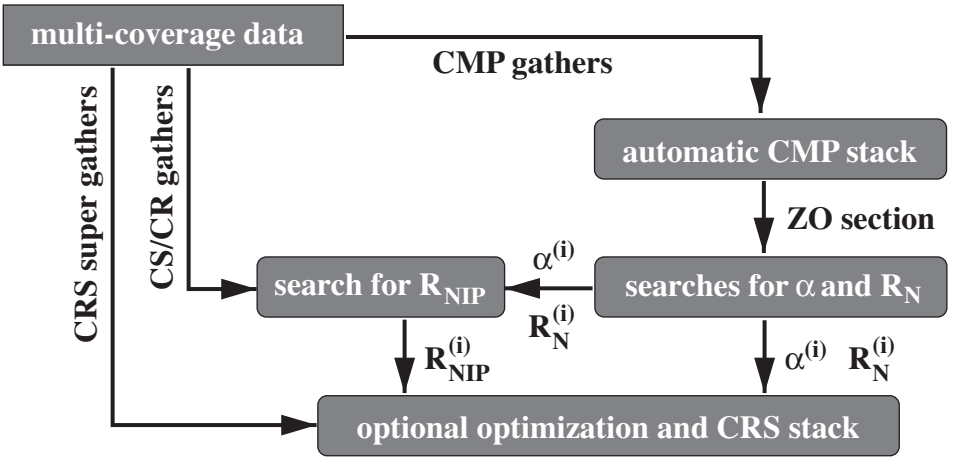

Fig. 3. Simplified flowchart of the extended CRS search strategy. The indicated processing steps have to be performed for each ZO sample to be simulated. All traces within the spatial CRS aperture are denoted as CRS super gather (from Mann, 2002).

THE CONCEPT OF THE CDS STACK OPERATOR

The so-called impulse response describes how a process maps a spike in the input data domain into the output data domain. For the DMO process in a homogeneous 2D medium, the impulse response is a semicircle (for $h = 0$) or an ellipse ($h \neq 0$) which is given by (Hale, 1991)

$$(t_0^2/t_{NMO}^2) + (x^2/h^2) = 1 \quad . \tag{3}$$

Each point on the DMO operator corresponds to a particular reflector dip. Thus, there is a relationship between the dip of the reflector and the slope measured on the DMO ellipse. Solving the equation above and differentiating with respect to x yields

$$x^2 - (vt_0/2\sin\phi)x - h^2 = 0 \quad , \tag{4}$$

with ϕ representing the reflector dip. This equation shows that the DMO operator provides the correct amount of lateral moveout for each dip. Since different parts of the DMO operator correspond to different dips, the conflicting dip problem is correctly handled, too.

In the CRS stack method, the same idea can be used to overcome the problem of conflicting dips. In this case, the reflector may have any arbitrary

curvature at the considered reflection point: we are not restricted to the DMO isochron, as the CRS concept considers the local reflector curvature. Just as for DMO, the actual number of conflicting events is not of interest here, because any present dip will contribute to the stack for the sample. However, the coherence analysis here also estimates how well the stacking operator fits the reflection event, although having a unique coherence section is impossible in this approach: A coherence analysis is performed for an entire range of angles for each sample. Thus, there are hundreds of different coherence values for each sample. Similar considerations also hold for the other wavefield attributes. Although not yet implemented, we might in future store the highest encountered coherence value and its associated attributes. In this way, we will know the characteristics of the best fitting operator out of the large number of employed operators.

CDS OPERATOR

In the ZO section, we often encounter intersections of reflection events and diffraction events. Solving the problem of conflicting dips will enhance the usually weak diffraction events in the stacked section. As the new strategy not only addresses reflection events but in particular diffraction events, we call it common-diffraction-surface (CDS) stack: For diffraction events, the radii of the NIP wavefront and the normal wavefront coincide, i.e., $R_{NIP} = R_N$. For reflection events, the two radii will in general differ. Nevertheless, we can use the traveltime approximation for a diffraction event to perform a stack. For reflection events, this implies a less accurate approximation than the full CRS operator (1). As a consequence, diffraction events will be enhanced compared to reflection events. Furthermore, the approximation for diffraction events contains less independent parameters: For a fixed emergence angle α, the only attribute to be searched for is a combined curvature called R_{CDS}. Thus, the traveltime approximation reduces to

$$t^2(x_m,h) = [t_0 + 2\sin\alpha(x_m - x_0)/v_0]^2 + [2t_0\cos^2\alpha/v_0R_{CDS}][(x_m - x_0)^2 + h^2] \quad . \tag{5}$$

For actual diffraction events, R_{CDS} coincides with R_{NIP} and R_N. For reflection events, R_{CDS} represents a weighted average of the now different radii R_{NIP} and R_N. This implies that fitting the approximate diffraction response (5) to a *reflection* event will not provide the approximate response of a *hypothetical* diffractor at the reflection point, i.e., a time migration operator. The latter is obtained if R_{CDS} coincides with the "true" R_{NIP}, irrespective of R_N (Mann et al., 2000; Mann, 2002). However, neither R_{NIP} nor R_N are separately determined in the CDS approach.

A sample in the ZO section will receive contributions of any possible optimum operator for each angle that we are searching for. By considering all possible angles in eq. (5), a set of operators will make a weighted volume instead of a single stacking surface for each ZO sample. This will enhance any weak reflection and diffraction events which were obscured by dominant coherent events in the previous strategy. In the CDS approach, we consider a large, constant number of different dips, i.e., an almost continuous dip, at each ZO sample, whereas the previous strategy only considers a small, discrete number of contributing CRS operators with different dips. This discrete number of dips will, in general, vary from sample to sample. This may lead to the incomplete simulation of interfering events and/or to artifacts.

IMPROVED SEARCH STRATEGY

The strategy used here differs from the pragmatic strategy (Müller, 1998) and the extended strategy (Mann, 2002) in its way to find the optimum wavefield attributes. As mentioned before, it is impossible to have any unique sections of kinematic wavefield attributes and associated coherence values. For this strategy, we require access to the entire prestack dataset from the very beginning, not only to a sub-domain of it: neither the automatic CMP stack nor the ZO search steps are suited to address this problem. Instead, the only option is to directly go through the whole data with the spatial operator (5) and to search for the only remaining variable, the attribute R_{CDS}.

The user should first define the range of considered emergence angles along with a suitable angle increment. The larger the search range the more computation time is needed to define the individual operators. Therefore, it is recommended to use a small range in areas with flat reflection events with little steep diffraction events, like the real land data that will be presented later on, and to choose a wider range in complicated situations with more conflicting dips and diffraction events, like in the Sigsbee 2A data. The target zone, the aperture, and the range for minimum and maximum stacking velocity are defined as for the pragmatic search strategy.

For the range of R_{CDS} values to be tested, the shape of the operator can be defined in terms of a moveout range. By coherence analysis, the optimum value of R_{CDS} can be calculated in the next step. Although this initial maximum could be further refined, this would be computationally very expensive and would have little impact on the final stack result. Now, by knowing the optimum value of R_{CDS} and the emergence angle α, eq. (5) defines the shape of the stacking operator for the specified sample. According to the user given angle increment $d\alpha$, the same procedure for the same sample is performed for the next defined angle ($\alpha + d\alpha$) within the angle range. This procedure is repeated over

the entire angle range. This whole procedure is applied for all ZO samples to be simulated. At the end, we receive a stacked section accompanied by a section containing the number of contributing traces within the respective aperture. Fig. 4 shows a simplified flowchart of the new improved strategy.

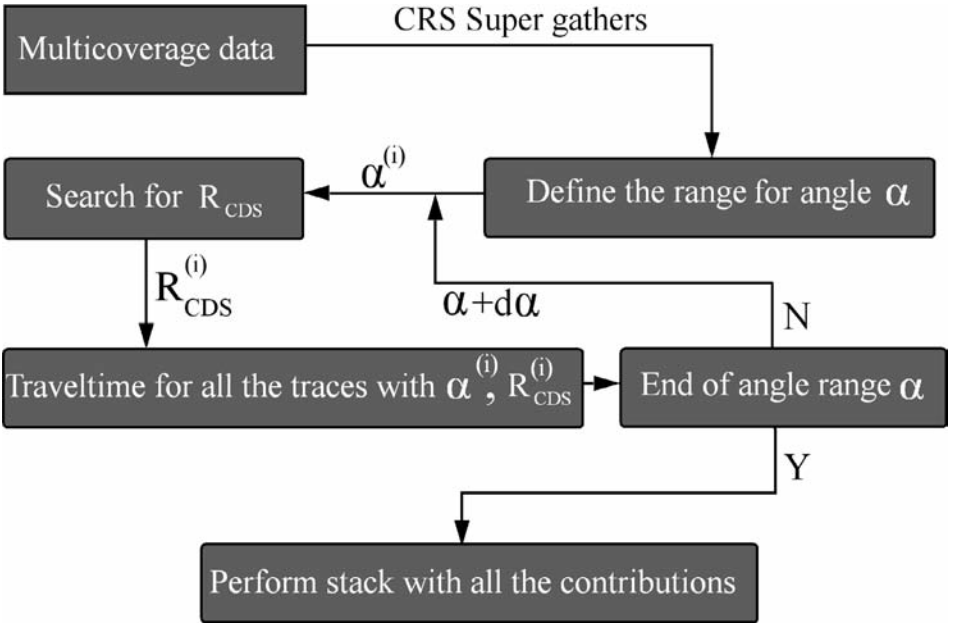

Fig. 4. Simplified flowchart of the improved strategy.

SYNTHETIC AND REAL DATA EXAMPLES

Sigsbee 2A synthetic data

The so-called Sigsbee 2A data is based on a stratified background model containing a salt body with a quite complicated geometry. Fig. 5 shows the CRS-stacked section for this model created with the extended search strategy. In the left part there are slightly dipping layers up to a time of 9 s ending with a strong reflection event. In the top right part there are also similar sedimentary structures which cover the salt body with its small syncline structure. Strong, extended diffraction patterns and bow-ties dominate the central part of the section whereas some weak diffraction events can also be seen in the left and lower parts of the section.

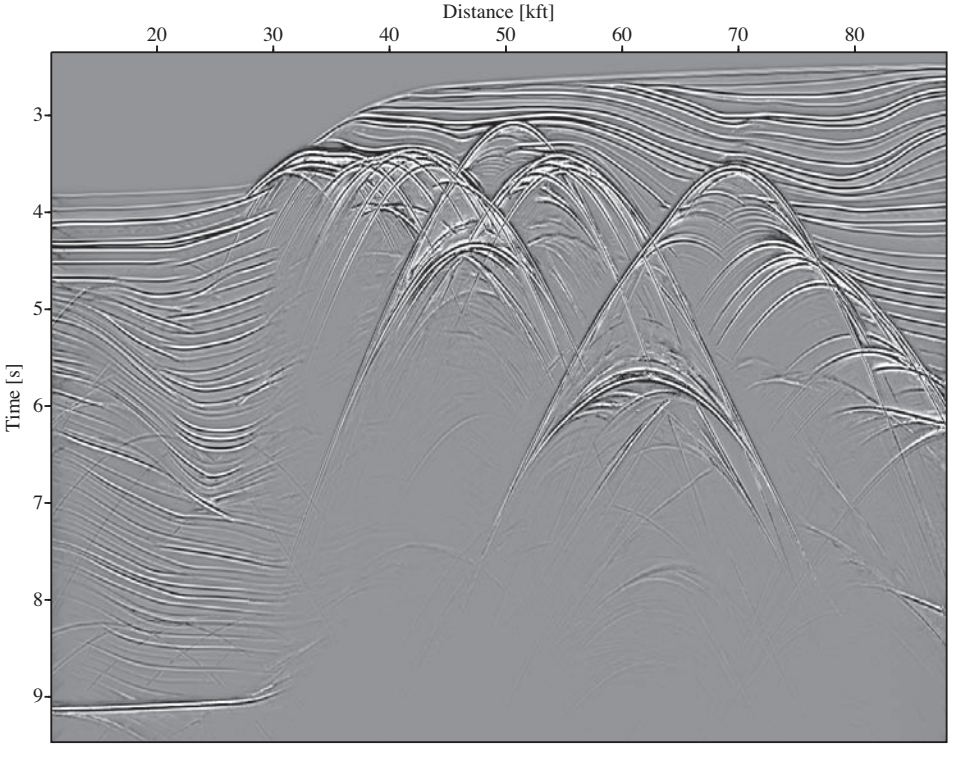

Fig. 5. CRS-stacked section of the Sigsbee 2A data (modified after Mann, 2002).

The result of CDS stacked section is shown in Fig. 6. Compared to the result of the CRS stack, as it could be seen at first glance, diffraction patterns are enhanced in all parts of the CDS stacked section. In particular in the sedimentary structures in the left-hand part, diffraction events which are partly or fully obscured by reflection events in the CRS stack section are clearly imaged. In the upper part, there are also many diffraction events in a regular pattern which are due to modeling effects. The lower right part of the CDS section has been omitted during processing to shorten the total computation time.

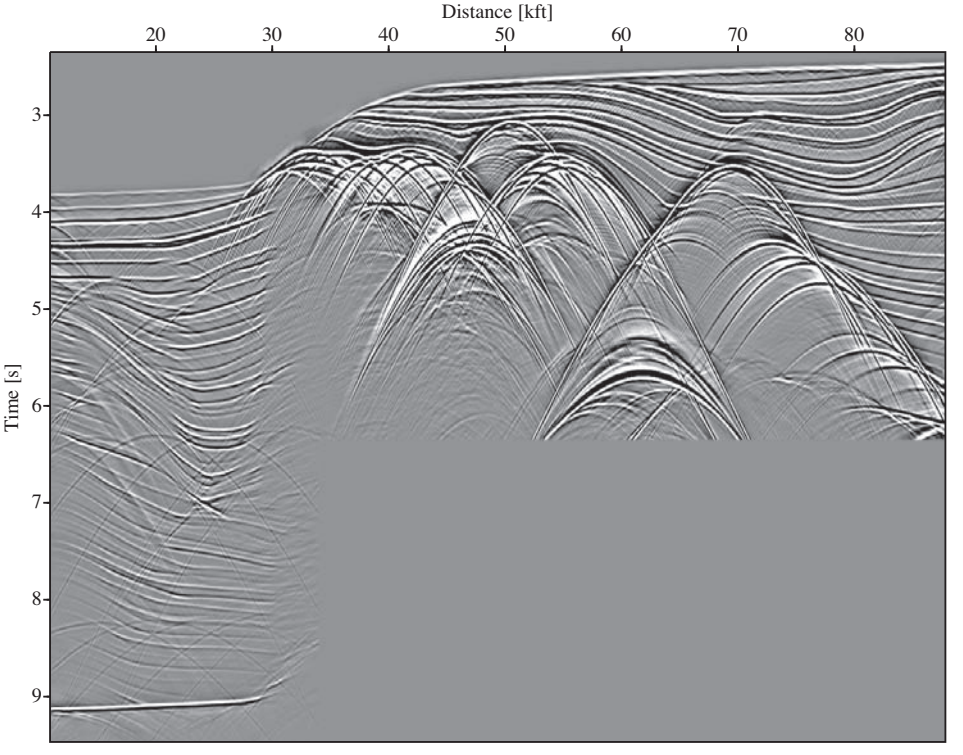

Fig. 6. CDS-stacked section of the Sigsbee 2A data.

To highlight the differences of the CDS stack result and the CRS stack results by Mann (2002), it is convenient to compare some subsets of the stacked sections. Fig. 7 shows the same subset of the two different results. In the section on the left-hand side, which is the result of the extended strategy, diffraction patterns are simulated but some of them have gaps where they intersect reflection events. These gaps correspond to locations where the conflicting dip situation has not been properly detected during the stack. In contrast, in the right-hand picture showing the result of the CDS stack, the continuity of these events is fully preserved and there are no gaps in the diffraction events, even where they intersect other events. Fig. 8 shows another subset of these stacked sections obtained with the two different methods. Again, the conflicting dips problem is better resolved in the CDS-stacked section than in the CRS-stacked section: all events contributing to the ZO samples are clearly defined.

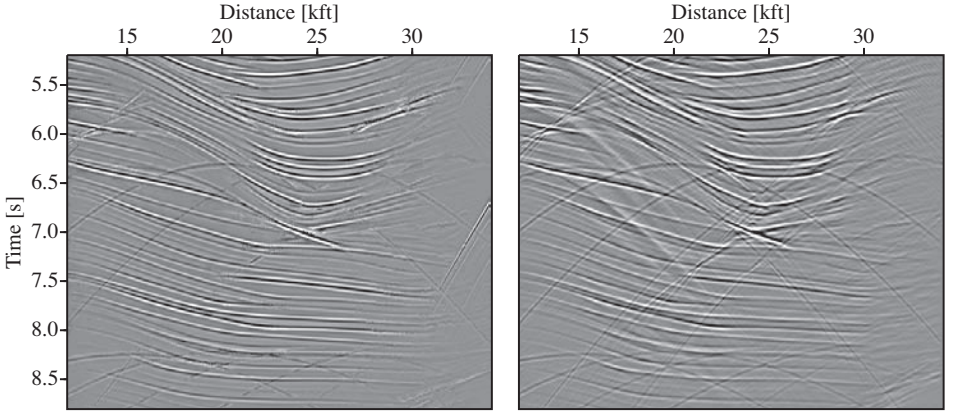

Fig. 7. Sigsbee 2A data: Details of the CRS-stacked result (left) and the CDS-stacked result (right).

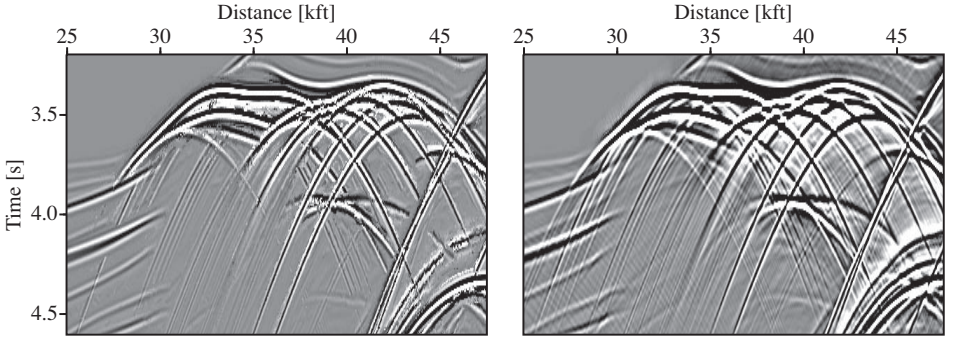

Fig. 8. Sigsbee 2A data: Details of the CRS-stacked result (left) and the CDS-stacked result (right).

Real land data example

The 2D seismic land dataset was acquired by an energy resource company in a fixed-spread geometry. The seismic line has a total length of about 12 km. The utilized source signal was a linear upsweep from 12 to 100 Hz of 10 s duration. Shot and receiver spacing are both 50 m and the temporal sampling interval is 2 ms. Standard preprocessing was applied to the field data including the setup of the data geometry, trace editing, deconvolution, geometrical spreading correction, field static correction, and bandpass filtering. The underlying structure consists of nearly horizontal layers disrupted by several faults.

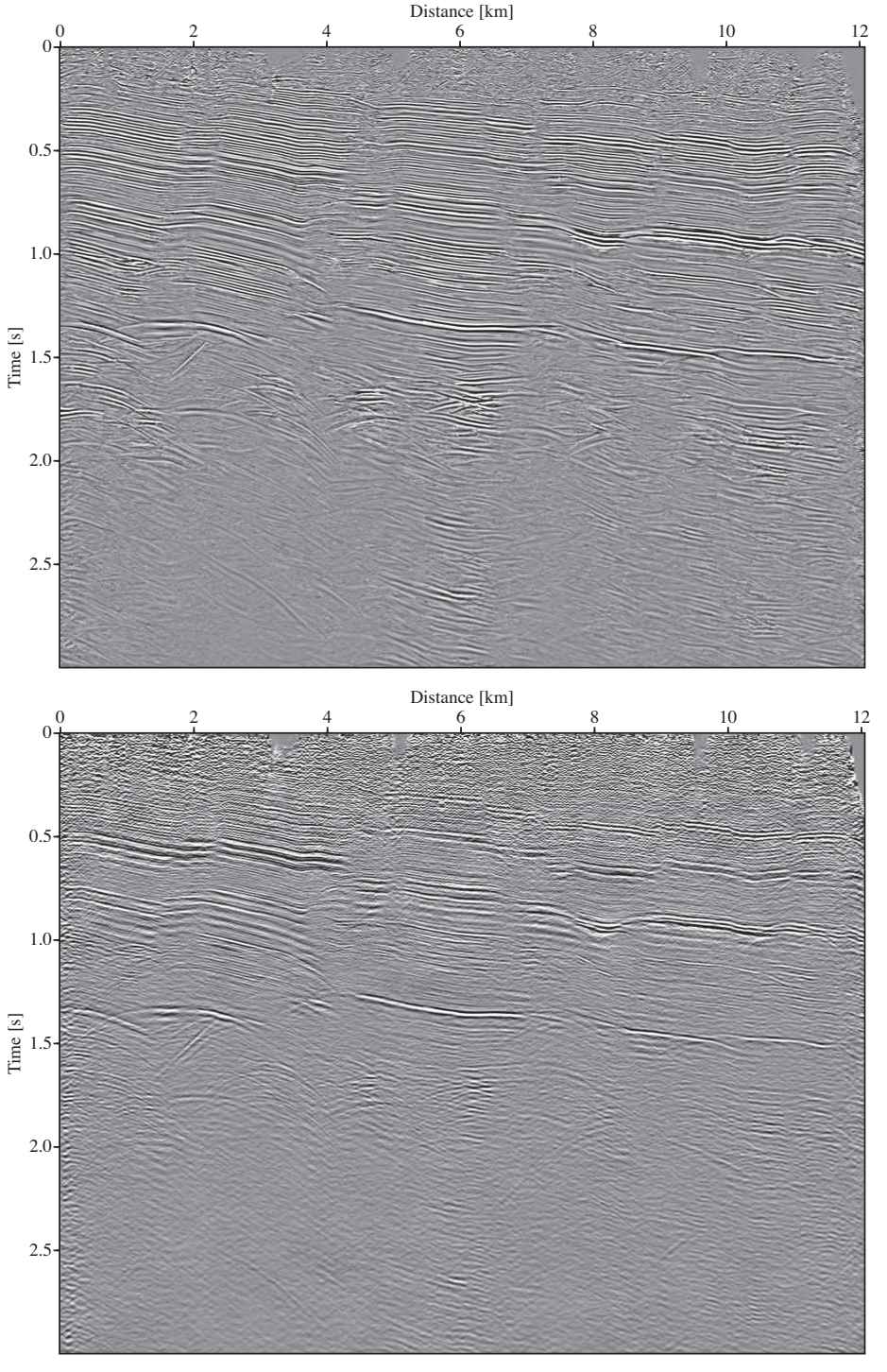

Fig. 9. Real land data: CRS-stacked section (top) and CDS-stacked section (bottom).

In CRS stack processing, mapping the position of faults, their boundaries, and their dips is difficult because the problem of conflicting dips exists here due to edge-diffractions at the faults. Fig. 9 shows the stacked sections obtained with the CRS method and the CDS method, respectively. The diffraction events are again emphasized and the faults are also clearer than in the pragmatic result, but that is not very evident from the stack sections, only.

A macro-velocity model for this data is available (see, e.g., Hertweck et al., 2004; Hertweck, 2004) such that poststack depth migration can be applied to compare the result with the result of the migrated CRS-stacked section. The traveltime tables were calculated using an eikonal solver and a Kirchhoff migration algorithm has been applied. The results are shown in Fig. 10, some significant differences are marked by arrows. To further highlight the differences between these two migrated sections, Fig. 11 shows two subsets of the results: the CDS result present a higher continuity of the events and a far better definition of the faults compared to the CRS result.

CONCLUSIONS

The pragmatic approach of Müller (1998) and the extended strategy of Mann (2002) have been combined with the concepts of DMO correction to handle the problem of conflicting dip situations. In this idea, not only the emergence angles satisfying the absolute and relative threshold coherence in the extended strategy, but all angles within a predefined range are explicitly considered to define a multitude of stacking operators for a ZO sample. In the new approach, the kinematic wavefield attributes are reduced to a combination of the radii of curvature of normal wave and NIP wave, called R_{CDS}, and the emergence angle is predefined on a regular grid. This approximation prefers diffraction events which, thus, are particularly emphasized compared to reflection events. The search for the attribute R_{CDS} is performed in one step in the whole dataset from the very beginning.

The result of applying the improved strategy to synthetic and real data demonstrated that this strategy is able to resolve the problem of conflicting dip situations and yields a stacked section with more continuous and clearer images of (previously obscured) weak events. The results of poststack depth migration of a real data also showed that the stacked section of the CDS stack is a suitable input for migration. The new operator collects more energy along weak events that might be lost in the previous strategies. This leads to an improved image quality at discontinuities and in faulted areas which improves the poststack migration result at such discontinuities. Therefore, the CDS stack method complements the conventional CRS-based imaging approach.

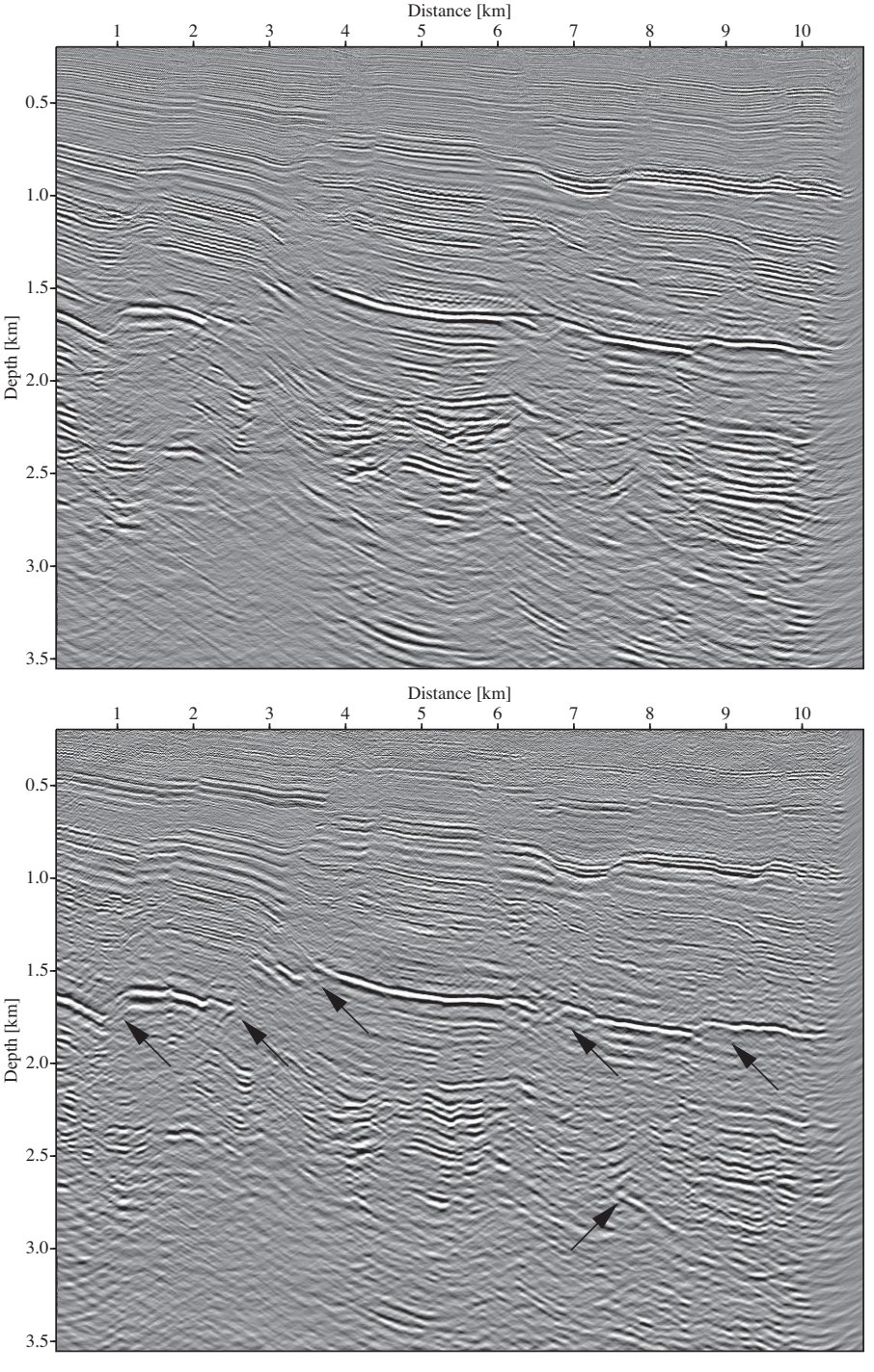

Fig. 10. Real land data: Poststack-migrated sections based on the CRS-stacked section (top) and the CDS-stacked section (bottom).

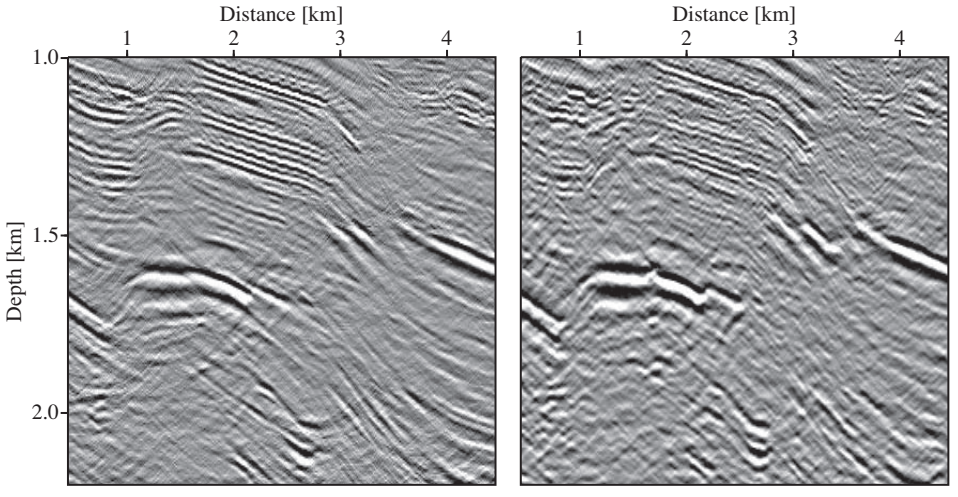

Fig. 11. Real land data: Details of the poststack-migrated sections based on the CRS-stacked section (left) and the CDS-stacked section (right).

ACKNOWLEDGMENTS

We would like to thank the sponsors of the Wave Inversion Technology (WIT) consortium for their support. We also thank Thomas Hertweck for the fruitful discussion and his detailed review. Finally, we thank Ines Veile for providing us with the depth migrated sections. The Sigsbee 2A data have been provided by the Subsalt Multiple Attenuation And Reduction Technology Joint Venture (SMAART JV).

REFERENCES

Hale, D., 1991. Dip Moveout Processing. SEG, Tulsa, OK.

Hertweck, T., 2004. True-amplitude Kirchhoff Migration: Analytical and Geometrical Considerations. Logos Verlag, Berlin.

Hertweck, T., Jäger, C., Mann, J., Duveneck, E. and Heilmann, Z., 2004. A seismic reflection imaging workflow based on the Common-Reflection-Surface (CRS) stack: theoretical background and case study. Expanded Abstr., 74th Ann. Internat. SEG Mtg., Denver: SP 4.3.

Hertweck, T., Schleicher, J. and Mann, J., 2007. Data-stacking beyond CMP. The Leading Edge, 26: 818-827.

Hubral, P. (Ed.), 1999. Macro-model Independent Seismic Reflection Imaging. J. Appl. Geophys., 42: 137-346.

Jäger, R., 1999. The Common Reflection Surface Stack - theory and application. M.Sc. thesis, University of Karlsruhe.

Jäger, R., Mann, J., Höcht, G. and Hubral, P., 2001. Common-Reflection-Surface stack: image and attributes. Geophysics, 66: 97-109.

Mann, J., 2001. Common-Reflection-Surface stack and conflicting dips. Extended Abstr., 63rd EAGE Conf., Amsterdam: P077.

Mann, J., 2002. Extensions and Applications of the Common-Reflection-Surface Stack Method. Logos Verlag, Berlin.

Mann, J., Höcht, G., Jäger, R. and Hubral, P., 1999. Common Reflection Surface stack - an attribute analysis. Extended Abstr., 61st EAGE, Helsinki: P140.

Mann, J., Hubral, P., Traub, B., Gerst, A. and Meyer, H., 2000. Macro-model independent approximative prestack time migration. Extended Abstr., 62nd EAGE Conf., Glasgow: B-52.

Müller, T., 1998. Common Reflection Surface stack versus NMO/stack and NMO/DMO/stack. Extended Abstr., 60th EAGE Conf., Leipzig: 1-20.

Müller, T., Jäger, R. and Höcht, G., 1998. Common Reflection Surface stacking method - imaging with an unknown velocity model. Expanded Abstr., 68th Ann. Internat. SEG Mtg., New Orleans: 1764-1767.

Nelder, J.A. and Mead, R., 1965. A simplex method for function minimization. Computer J., 7: 308-313.